Anal. Chem. **2008,** *80,* 8299–8307

Continuous Time-of-Flight Ion Imaging: Application to Fragmentation

Oh Kyu Yoon, Matthew D. Robbins, Ignacio A. Zuleta, Griffin K. Barbula, and Richard N. Zare*

Department of Chemistry, Stanford University, Stanford California 94305-5080

We have designed and constructed a continuous imaging reflectron time-of-flight mass spectrometer (TOFMS) that provides a mass spectrum at every pixel of a two-dimensional image with a 100% duty cycle. The technique is based on pseudorandom ion beam modulation and three-dimensional (*x*, *y*, *t*) ion imaging. We use a multichannel plate detector with a delay-line anode that provides *x*, *y* positions and flight times *t* of every ion arrival event. The precision of the peak heights in the 100% duty cycle mass spectra is shown to be enhanced even at short (10 ms) acquisition times, which should prove useful for the study of solution kinetics or fast chromatographic separations. As a demonstration of the system's capability, we have imaged the fragmented ions that underwent surface-induced dissociation inside the reflectron and the ions that fragmented spontaneously through postsource decay.

Recent growth in mass spectrometry (MS) has been driven by the development of soft ionization methods, such as matrix-assisted laser desorption ionization (MALDI)[1] and electrospray ionization (ESI).[2] These techniques enable the analysis of more complex samples, especially those of biological interest. In a typical MS experiment, analyte ions are physically separated or filtered according to their mass-to-charge (m/z) ratio based upon some parameter, such as flight time, position, or kinetic energy, that is accessible by controlling an electric or magnetic field. The m/z ratio of detected ions is inferred by correlating the field control to the response of a one-dimensional (1D) detector such as a photomultiplier tube, multichannel plate (MCP), or channeltron. In Fourier transform mass spectrometry,[3] m/z ratios map to the cyclotron frequencies of the ions, and the measured image current is deconvoluted. Recent advances in two-dimensional (2D) imaging detectors have allowed researchers to explore their use in MS. The main advantages of multidimensional detection are the increased information content that results from making simultaneous measurements of multiple parameters and the potential to exploit the high-throughput (Jacquinot) advantage[4] that leads to a higher signal-to-noise ratio (SNR) and reduced analysis time for some systems. One example of 2D detection is the use of photographic plates[5] or array detectors[6−8] in the implementation of a Mattauch−Herzog double focusing mass spectrometer. This instrumental configuration allows the simultaneous detection of individual ion currents in the detector plane. In chemical physics experiments, MCP detectors coupled to phosphor screens followed by charge-coupled devices (CCD) have been used in velocity map imaging MS[9,10] to measure the velocity distributions of different species in bimolecular chemical reactions and unimolecular photodissociation experiments.[11] Recently, three-dimensional (3D) delay line detectors have been employed to study bimolecular reactions, where the detector enables the measurement of all three components of the velocity distribution from the reaction products.[12,13]

We report here the development of a continuous imaging reflectron time-of-flight mass spectrometer (TOFMS) that provides a mass spectrum at every pixel of a 2D image with 100% duty-cycle. Compared to a conventional reflectron TOFMS, which couples to a continuous ion source such as ESI by pulsing the ion beam into the mass analyzer, the imaging TOFMS time-stamps the beam by pseudorandom beam modulation and employs a 3D (*x*, *y*, *t*) imaging detector. The imaging detector used is a multichannel plate (MCP) with a delay-line anode[14] that provides positions *x*, *y* and flight time *t* of every ion arrival event (Figure 1b). The delay-line anode consists of two orthogonal sets of wires, where each set is composed of a signal wire and a reference wire. When an ion arrives at the MCP detector, an electron cloud is produced which is collected by the wire sets and induces two electric current pulses to travel to the ends of each wire. The arrival times of the two pulses at the end of each wire set encode the position and absolute arrival time of an ion arrival event. In this scheme the difference in detected arrival times gives the ion arrival position in one dimension, and the average of the two

* To whom correspondence should be addressed. E-mail: zare@stanford.edu.

(1) Tanaka, K.; Waki, H.; Ido, Y.; Akita, S.; Yoshida, Y.; Yoshida, T.; Matsuo, T. *Rapid Commun. Mass Spectrom.* **1988**, *2*, 151–153.
(2) Fenn, J. B. *Angew. Chem., Int. Ed.* **2003**, *42*, 3871–3894.
(3) Marshall, A. G.; Hendrickson, C. L.; Jackson, G. S. *Mass Spectrom. Rev.* **1998**, *17*, 1–35.
(4) Griffiths, P. R. *Science* **1983**, *222*, 297–302.
(5) Mattauch, J.; Herzog, R. F. K. *Z. Phys.* **1934**, *89*, 789.
(6) Nier, A. O.; Hayden, J. L. *Int. J. Mass Spectrom. Ion Phys.* **1971**, *6*, 339.
(7) Schilling, G. D.; Andrade, F. J.; Barnes, J. H.; Sperline, R. P.; Denton, M. B.; Barinaga, C. J.; Koppenaal, D. W.; Hieftje, G. M. *Anal. Chem.* **2007**, *79*, 7662–7668.
(8) Barnes, J. H.; Hieftje, G. M. *Int. J. Mass Spectrom.* **2004**, *238*, 33–46.
(9) Kim, M. H.; Leskiw, B. D.; Suits, A. G. *J. Phys. Chem. A* **2005**, *109*, 7839–7842.
(10) Kim, M. H.; Leskiw, B. D.; Shen, L.; Suits, A. G. *Int. J. Mass Spectrom.* **2006**, *252*, 73–78.
(11) Tsai, S.-T.; Lin, C.-K.; Lee, Y. T.; Ni, C.-K. *Rev. Sci. Instrum.* **2001**, *72*, 1963–1969.
(12) Koszinowski, K.; Goldberg, N. T.; Pomerantz, A. E.; Zare, R. N. *J. Chem. Phys.* **2006**, *125*, 133503.
(13) Hanold, K. A.; Luong, A. K.; Clements, T. G.; Continetti, R. E. *Rev. Sci. Instrum.* **1999**, *70*, 2268–2276.
(14) Jagutzki, O.; Mergel, V.; Ullmann-Pfleger, K.; Spielberger, L.; Spillmann, U.; Dörner, R.; Schmidt-Böcking, H. *Nucl. Instrum. Methods Phys. Res. A* **2002**, *477*, 244–249.

10.1021/ac801512n CCC: $40.75
Published on Web 10/07/2008

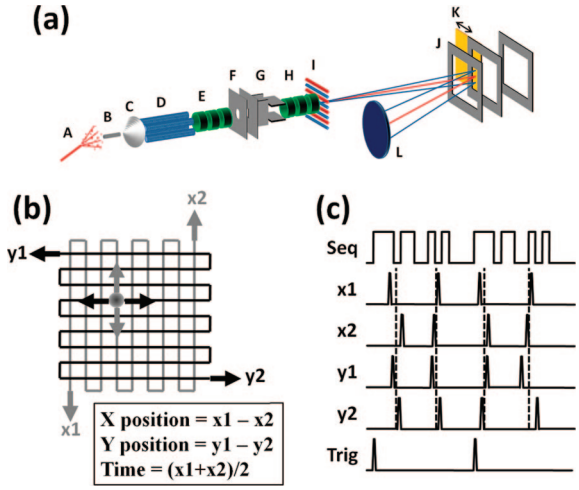

Figure 1. Schematic of the continuous imaging HT-TOFMS instrument. (a) The instrument is composed of electrospray ion source (A), heated capillary (B), skimmer (C), quadrupole rf-only ion guide (D), low-voltage einzel lens (E), acceleration region (F), deflection plates (G), high-voltage einzel lens (H), Bradbury–Nielsen gate (I), double-stage reflectron (J), surface for surface-induced dissociation (K), and imaging detector (L). (b) A schematic of the delay line anode. An ion arrival at the multichannel plates will be amplified into an electron cloud that is collected by the two orthogonal wire sets. In each wire, the electron cloud induces two current pulses that travel to the two ends of the wire sets. The difference in arrival time of the two pulses encodes the position and the average encodes the flight time. (c) The timing diagram of the Hadamard sequence, four delay line signals, and the trigger signal.

arrival times gives the absolute ion arrival time with a constant offset. Using this information from the two orthogonal wire sets, the two-dimensional positions, *x* and *y*, and the arrival time, *t*, of each ion can be measured.

This experiment achieves 100% duty cycle through ion beam modulation in a manner similar to two-channel (2C) Hadamard transform (HT) TOFMS, in which a patterned MCP anode was used for detection.[15] The principle of HT-TOFMS has been described previously.[15–17] Briefly, a continuous ion beam is deflected on and off the axis of its initial trajectory at rates of tens of megahertz using a Bradbury–Nielsen gate (BNG)[18] according to a pseudorandom binary sequence known as a Hadamard sequence. In contrast, in a conventional linear TOFMS experiment used to study a continuous source, a single ion packet is generated by pulsing the ion beam into the mass analyzer. That packet must be completely analyzed before another ion packet is introduced into the analyzer. As a result, the duty cycle of this experiment is low. In HT-TOFMS, analogous packets are continuously introduced and thousands of such packets are analyzed and detected in the time it takes one packet to go from the BNG to the detector. Thus, the signal at the detector is a sum of thousands of time-shifted mass spectra. From the knowledge of the sequence used to modulate the ion beam, the detected signal can be deconvoluted to obtain a mass spectrum with increased SNR. The Hadamard sequences used are composed of approximately half 1 s and half 0 s, leading to a 50% duty cycle for experiments detecting either undeflected or deflected ions. However, by measuring both the undeflected and the deflected beams, a 100% duty cycle can be achieved. Although 100% duty cycle was theoretically possible in the 2C-HT-TOFMS experiment described previously, this detection method required exactly matching the beam dimensions and the deflection distance to the detector dimensions. The requirement proved difficult to achieve in practice and resulted in some reduction of the duty cycle. In the imaging HT-TOFMS scheme implemented here, true 100% duty cycle is achieved for every experiment. The observed SNR can be maximized by choosing the best windows during the data processing, which removes correlated noise between them. In addition, the data can be binned into pixels to directly image the ion beam profiles as a function of m/z ratios. Thus, the mass spectral image can resolve different chemical or physical processes in the ion beam.

As an application of this new capability to spatially resolve ion phenomena, we have imaged the fragment ions from surface-induced dissociation (SID) and from postsource decay (PSD). Different fragmentation processes are dispersed along the *x*-axis in the reflectron due to a combination of their kinetic energies, flight times, and interactions with the SID surface, which is located inside the reflectron. The ion beams are modulated using a BNG by deflecting along the *y*-axis, and the time axis provides the chemical identity of the fragments through their m/z ratios. Thus, this application demonstrates the use of all three dimensions, *x*, *y*, and *t*. Different fragmentation processes show different correlations between *x* and *t*, offering a means for separating and studying reactions within a mass spectrometer.

EXPERIMENTAL SECTION

Imaging Hadamard Transform Reflectron Time-of-Flight Mass Spectrometer. Figure 1a presents a schematic diagram of the home-built ion imaging mass spectrometer. The electrospray ion source (A) was salvaged from a Mariner TOFMS (PerSeptive Biosystems, Framingham, MA), which contains a heated capillary (B), skimmer (C), quadrupole rf-only ion guide (D), and low-voltage ion optics (E). The ion guide was operated at 700 kHz using a home-built variable-frequency variable-amplitude rf power supply.[19] The collimated ion beam was accelerated by 1.5 kV (F) and then recollimated using deflection plates (G) and a high-voltage einzel lens (H). The BNG (I) was fabricated using 10 μm outer diameter gold-plated tungsten wires (California Fine Wires, Grover Beach, CA) at a wire spacing of 100 μm.[18] BNG voltages of ±10 V relative to the field-free region were applied to the BNG wires. The Hadamard sequences were generated in low-voltage differential logic (LVDL) using a 50 MHz digital waveform generator/analyzer (PCI-6551, National Instruments, Austin, TX) and were input to a custom-designed BNG driver circuit.[20] The home-built two-stage reflectron (J) consisted of 21 electrodes with a spacing of 10 mm. All electrodes had an active area of 40 mm by 70 mm, and the first, sixth, and last electrodes were covered with 90% transmission Ni mesh (BM0070-01, Buckbee Mears, St.

(15) Trapp, O.; Kimmel, J. R.; Yoon, O. K.; Zuleta, I. A.; Fernandez, F. M.; Zare, R. N. *Angew. Chem., Int. Ed.* **2004**, *43*, 6541–6544.
(16) Kimmel, J. R.; Yoon, O. K.; Zuleta, I. A.; Trapp, O.; Zare, R. N. *J. Am. Soc. Mass Spectrom.* **2005**, *16*, 1117–1130.
(17) Yoon, O. K.; Zuleta, I. A.; Robbins, M. D.; Barbula, G. K.; Zare, R. N. *J. Am. Soc. Mass Spectrom.* **2005**, *16*, 1888–1901.
(18) Yoon, O. K.; Zuleta, I. A.; Robbins, M. D.; Barbula, G. K.; Zare, R. N. *J. Am. Soc. Mass Spectrom.* **2007**, *18*, 1901–1908.
(19) Robbins, M. D.; Yoon, O. K.; Zuleta, I. A.; Barbula, G. K.; Zare, R. N. *Rev. Sci. Instrum.* **2008**, *79*, 034702.
(20) Bolton, C. *Electronic Design News (EDN)*, October 3, **2002**, *88*.

Paul, MN). The SID surface (K) was attached to the 13th electrode and can be translated in and out of the ion path using a linear manipulator. The reflectron is tilted horizontally by 4° relative to the entrance propagation direction of the ions. The detector (L) consisted of two 80 mm MCP plates and a delay-line anode (DLD80, RoentDek Handels GmbH, Kelkheim-Ruppertshain, Germany). The front of the MCP plates was at −2200 V. The length of the first field-free region between the BNG and the reflectron is 1.3 m, and the length of the second field-free region between the reflectron and the detector is 0.65 m. The pressures at the heated capillary, rf-only ion guide, the BNG, and the flight chamber were typically 10 Torr, 100 mTorr, 5×10^{-7} Torr, and 1×10^{-7} Torr, respectively. As shown in Figure 1b, the delay-line anode consists of two orthogonal sets of wires (x and y axes), where each set has a signal wire and a reference wire (reference wire not shown in Figure 1b). The signal and reference wires were at 306 and 270 V, respectively, so that electrons will be preferentially collected by the signal wires. The four differential signals (x1, x2, y1, and y2) between the signal and the reference wires are RC decoupled and impedance matched using an FT12-TP feedthrough (RoentDek) and then are processed with constant-fraction discriminators and converted to four single-ended NIM pulses using an amplifier-discriminator module (ATR-19, RoentDek). A trigger pulse is also output from the sequence generator PCI-6551 at the start of every Hadamard sequence and converted to NIM logic with a delay generator (DG535, Stanford Research Systems, Sunnyvale, CA). The five NIM signals are input to a time-to-digital converter TDC8HP (RoentDek). Figure 1c shows a schematic diagram of the five signals. CoboldPC data acquisition software (RoentDek) was used for operation and data acquisition of the delay-line detector, which outputs a list of x1, x2, y1, y2, and arrival times of all ions as a list-mode format (LMF) file.

Data Processing. Data processing programs were written using Python.[21] This software converts the LMF file (output file from CoboldPC data acquisition software) to a hierarchical data format (HDF5) file,[22] which is a standard format for large data handling. During the conversion, the list of x1, x2, y1, y2, and arrival times were converted to a list of x, y positions and flight times, which were rereferenced relative to the trigger signal from the sequence generator (PCI-6551). Typically, a few percent of the data were missing some of the four delay-line signals, and these "missing events" were removed from the list. The ion information from the HDF5 file was used to create a 3D histogram of x, y positions and times t, perform a Hadamard deconvolution along the time axis, and plot 1D, 2D, or 3D images of the deconvoluted data. Typically, the size of our LMF files are a few hundred megabytes, but the resulting HDF5 files are 5−8 times smaller.

Surface-Induced Dissociation. A self-assembled monolayer of 2-(perfluorodecyl)ethanethiol was formed on a gold-plated stainless steel plate (50 mm × 70 mm × 0.5 mm). Self-assembled monolayers of alkane thiol species have been shown to enhance the fragmentation yield in SID experiments.[23] The coated stainless steel plate is attached to the 13th electrode in the two-stage reflectron. The surface is connected to a linear manipulator (660008, MDC Vacuum Products, Hayward, CA) and can be translated in and out of the ion path within the reflectron. A SimIon[24] simulation shows that the field distortion from surface insertion is minimal (data not shown). The collision energy of the surface-induced dissociation can be varied by changing the reflectron voltage settings. The collision voltage is calculated as the difference between the acceleration voltage and the voltage on the SID electrode. The collision energy can be calculated by the sum of the initial kinetic energy before acceleration and the collision voltage multiplied by the charge. A collision voltage of 30 V for a triply charged ion should correspond to a collision energy of about 90 eV.

Chemical Samples. The concentrations of bradykinin (American Peptide, Sunnyvale, CA), rhodamine 6G (Sigma-Aldrich, St. Louis, MO), reserpine (Sigma-Aldrich), and angiotensin I (American Peptide) used in all experiments were 10 μM in a 50:50 vol/vol mixture of high-purity water (18 MΩ cm^{-1}) and methyl alcohol (Sigma-Aldrich) acidified with the addition of 1% by volume of acetic acid (Sigma-Aldrich). Analytes and solvents were used as received without further purification.

RESULTS AND DISCUSSION

Duty Cycle and Modulation Efficiency. The imaging Hadamard transform time-of-flight mass spectrometer spatially modulates a continuous stream of ions with a BNG and records the x, y positions and flight times of all ions that arrive at the MCP detector with a delay-line anode. Thus, the imaging HT-TOFMS has a 100% duty cycle. Although 2C-HT-TOFMS[15] can provide a 100% duty cycle, the two-channel detector dimensions were fixed and the ion beam dimensions and the deflection distance had to be matched to get a 100% duty cycle. This task was often challenging and would lead to reduced duty cycle when the instrument was not fully optimized. The use of an imaging detector to visualize the deflected ion beam facilitates the optimization significantly, and good separation of the deflected beams is easily achieved.

One of the requirements of HT-TOFMS is well-defined ion beam modulation. If the duty cycle is very high but the modulation is poor, the unmodulated ions will only contribute to baseline noise and the peak heights will be reduced. This concept is shown in the following two equations for the peak height and the variance of the baseline noise in each channel:[16]

$$z_{i,j} = \varepsilon_j F_i f_j^{\mathrm{HT}} \Psi_{\mathrm{Tot}} = \varepsilon_j F_i \Psi_j \tag{1}$$

$$\mathrm{Var}(z_{b,j}) = f_j^{\mathrm{HT}} \Psi_{\mathrm{Tot}} = \Psi_j \tag{2}$$

Here, Ψ_{Tot} is the total number of ions entering the TOFMS, Ψ_j is the number of ions in channel j, f_j^{HT} is the duty cycle of channel j in Hadamard mode, $z_{i,j}$ is the average peak height of species i in channel j, $z_{b,j}$ is the average peak height of the baseline in channel j, ε_j is the modulation efficiency in channel j, and F_i is the fraction of analyte i in the ion stream. The modulation efficiency is typically less than 100% because of the residence time through the BNG and the imperfections in modulation such as risetime and overshoot. The modulation efficiency in channel j can be calcu-

(21) Yoon, O. K. Ph.D. Thesis, Stanford University, Stanford, CA, 2008.
(22) http://hdf.ncsa.uiuc.edu/HDF5/index.html.
(23) Morris, M. R.; Riederer, D. E.; Winger, B. E.; Cooks, R. G.; Ast, T.; Chidsey, C. E. D. *Int. J. Mass Spectrom. Ion Processes* **1992**, *122*, 181–217.
(24) Dahl, D. A. *Int. J. Mass Spectrom.* **2000**, *200*, 3–25.

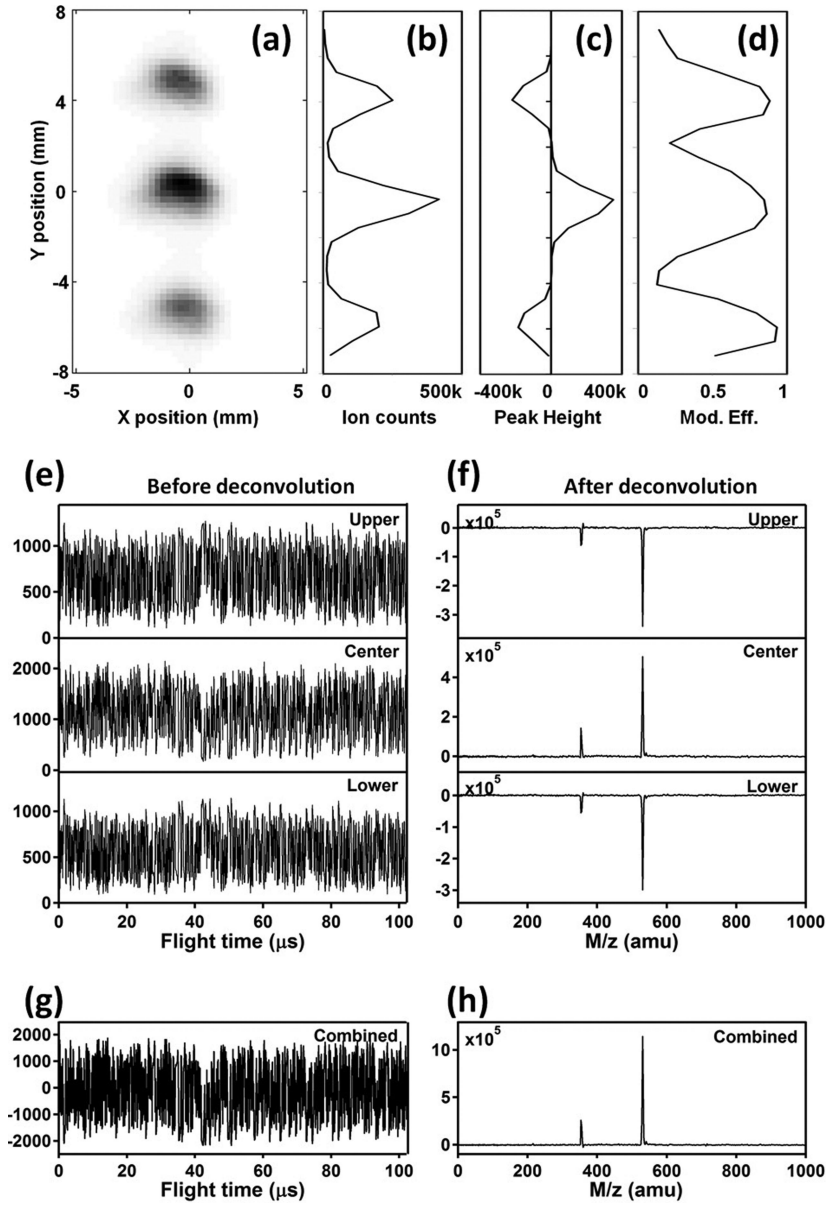

Figure 2. Modulation efficiency and mass spectra of bradykinin. (a) *xy* image of the three ion beam branches from modulation by the Bradbury−Nielsen gate. The (0,0) position in this plot has been referenced to the center of the ion beam and does not correspond to the center of the detector. (b) Total ion counts as a function of *y* position. (c) Sum of peak heights of +2 (531 amu) and +3 (354 amu) charges states of bradykinin. (d) Modulation efficiency calculated using eq 3. (e) Flight time data of the upper, center, and lower branches. (f) The mass spectra of the raw data in part e after Hadamard deconvolution. Parts g and h are the combined data calculated by taking the difference between the mass spectra for the undeflected (center) and deflected (upper and lower) beams.

lated by summing the peak heights of all analytes and then dividing by the ion counts in channel *j*:

$$\varepsilon_j = \left| \frac{\sum_i z_{i,j}}{\Psi_j} \right| \qquad (3)$$

Figure 2a is a 2D image (summed over time) of bradykinin ion counts modulated at 10 MHz with a Hadamard sequence of length 1023 showing the beam size, shape, and spatial separation of the center and the two deflected ion beam branches. The total ion counts as a function of *y* position are shown in Figure 2b, where the data were summed over *x* position and binned into 24 channels. The raw data in each channel can be deconvoluted with the Hadamard sequence to obtain mass spectra, which show the presence of +2 (531 amu) and +3 (354 amu) charge states of bradykinin. The sum of peak heights of the two charge states of bradykinin as a function of *y* position are shown in Figure 2c. The negative intensities in the upper and lower channels indicate that they were modulated by the complementary Hadamard sequence (0 and 1 switched) because when the BNG is "on," corresponding to state 1, the ions are "off," corresponding to state 0 in the deflected beams and vice versa. The modulation efficiency as a function of *y* position is calculated using eq 3 as a function of *y* position and the results are shown in Figure 2d.

Three 2D windows can be chosen for the three branches based upon regions of high modulation efficiency to get histograms of ion arrival events within the range of flight times corresponding

to one Hadamard sequence (Figure 2e). Mass spectra after deconvolution and mass calibration are shown in Figure 2f. The SNRs of the upper, center, and lower channels are 448, 475, and 445, respectively. The 100% duty cycle raw data and mass spectrum are obtained by taking the difference between the center and the deflected channels and they are also shown in the figures. The SNR for the combined spectrum (parts g and h of Figure 2) is 808, which is 1.7 times that of the center channel. This value is a bigger improvement in SNR than the previously reported value of 1.29. Moreover, it is larger than 1.41 ($\sqrt{2}$) that would arise from counting statistics alone if both channels have equal modulation efficiencies.[15] This SNR enhancement can be mostly attributed to a better choice of windows for the three channels such that the correlated noise components between the channels are removed. The peak height of the combined spectrum is equal to the sum of the absolute values of the peaks heights from the three channels. However, the variance of the baseline noise in the combined spectrum is about 90% of the sum of the variances of the three channels, indicating that 10% of the baseline noise has been removed.

Improvements in Peak Height Precision. The Hadamard sequence is generated using a high-speed digital output card PCI-6551, which can output arbitrary sequences. Thus, we have made a comparison between conventional and Hadamard mode acquisition in the same instrument. The Hadamard sequence of length 2047 was used at a 10 MHz modulation rate. To simulate a conventional mode experiment using the same 10 MHz modulation rate, a new sequence was created in which all sequence elements except the first element were set to zero. Note that this is not a comparison to orthogonal extraction OE-TOFMS,[25] which is commonly used for continuous ion sources in commercial instruments. The duty cycle of OE-TOFMS is typically between 5 to 50% and is dependent on the mass range (through the pulse repetition frequency) and mass-to-charge ratio (through the residence time).[26]

The mass spectra of a mixture of rhodamine 6G (479 amu) and reserpine (609 amu) are shown in Figure 3. The mass spectra were taken for acquisition times of 1 s (Figure 3a,b), 100 ms (Figure 3c,d), and 10 ms (Figure 3e,f) in Hadamard (Figure 3a,c,e) and conventional (Figure 3b,d,f) modes. The experiments were repeated 16 times to obtain the error bar in the peak heights. The SNR is normally calculated by dividing the peak height by the baseline noise. For the mass spectra acquired for 1 s, SNRs of the Hadamard and conventional mode are 142 and 39 for rhodamine 6G, and 113 and 43 for reserpine. This is an improvement of only 3−4 times. The theoretical SNR enhancement under signal-independent noise condition (Fellgett advantage) is $(2047)^{1/2}/2 = 23$.[27]Under signal-dependent noise conditions, the baseline noise for the conventional mode should be zero and the theoretical SNR enhancement is infinity. In reality, the conventional mode SNR is determined by chemical and detector noise whereas the Hadamard SNR is determined by the ion count statistics. The SNR enhacement is reduced for Hadamard mode in the presence of multiple peaks, because the baseline noise increases with the total ion counts caused by the shot noise from the ion count statistics.[16]

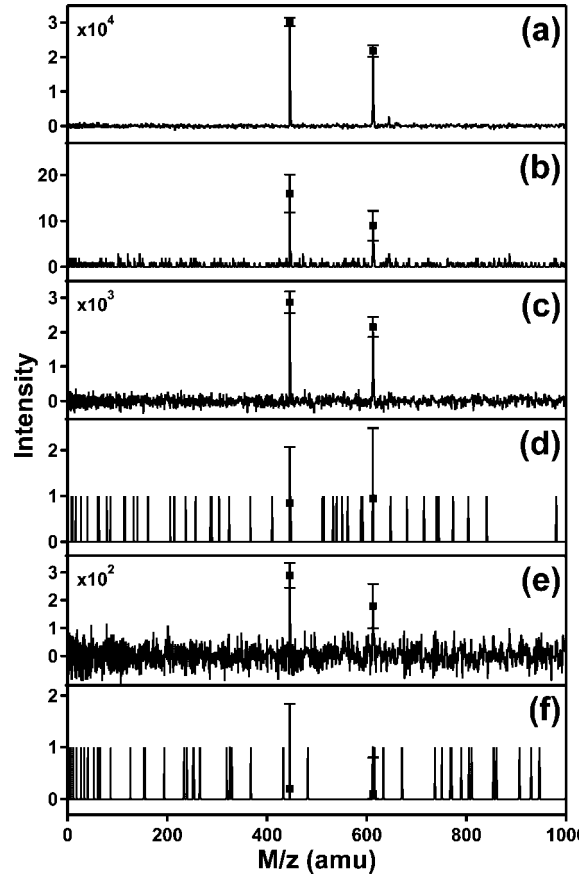

Figure 3. Peak height precision of rhodamine 6G (479 amu) and reserpine (609 amu) showing the spectral acquisition (a) of 1 s in Hadamard mode; (b) of 1 s in conventional mode; (c) of 100 ms in Hadamard mode; (d) of 100 ms in conventional mode; (e) of 10 ms in Hadamard mode; and (f) of 10 ms in conventional mode. The error bars are calculated from 16 experiments. Each plot is for one representative spectrum, and dots represent the average peak heights.

For ion counting experiments under signal-dependent noise conditions, a better figure of merit for comparison is peak height precision (PHP)[16] because PHP is mainly determined by the ion count statistics for both conventional and Hadamard mode experiments. PHP is defined as the peak height divided by its own standard deviation over many experiments. High PHP is important when the peak height is used for quantitation in experiments such as solution kinetics or coupling with chromatography techniques. In the shot-noise limit, the multiplexing advantage in peak height precision is given by[16]

$$\frac{\mathrm{PHP}_i^{\mathrm{HT}}}{\mathrm{PHP}_i^{\mathrm{Conv}}} = \varepsilon\sqrt{\frac{f^{\mathrm{HT}}}{f^{\mathrm{Conv}}}F_i} \qquad (4)$$

where $\mathrm{PHP}_i^{\mathrm{HT}}$and $\mathrm{PHP}_i^{\mathrm{Conv}}$ are PHPs of analyte i in Hadamard and conventional modes.

The standard deviations of the peak heights are shown as vertical error bars in Figure 3a,b for an acquisition time of 1 s. As shown by the error bars, the peak heights are more stable in the Hadamard mode compared to the conventional mode. Hadamard

(25) Guilhaus, M.; Selby, D.; Mlynski, V. *Mass Spectrom. Rev.* **2000**, *19*, 65–107.
(26) Boyle, J. G.; Whitehouse, C. M. *Anal. Chem.* **1992**, *64*, 2084–2089.
(27) Harwit, M.; Sloane, N. J. *Hadamard Transform Optics*; Academic Press: New York, 1979.

mode PHPs are 41 and 23 for rhodamine 6G and reserpine, respectively. Conventional mode PHPs are 4 and 3 for rhodamine 6G and reserpine. This comparison represents an improvement of about 10 times in PHP, which is smaller than the theoretical improvement of $0.9(2047)^{1/2} = 40$ under shot-noise limited conditions. The deviation from the theoretical improvement value is mainly due to fluctuations in the electrospray current, which is not taken into account in the theoretical derivation and the effects of imperfect beam modulation.

As the acquisition time is reduced such that the effects of ion statistics become dominant, the PHP improvement is very useful as shown in Figure 3c,d for an acquisition time of 100 ms. For the conventional mode, there are not enough ions to observe a mass spectrum, whereas in the Hadamard mode, the peak heights are still very stable. The PHPs of rhodamine 6G and reserpine are 15 and 18 for Hadamard mode and 1.1 and 1.7 for conventional mode. This improvement in PHP of 14 and 11 is still less than the shot-noise limit theoretical value of 40. This effect is even more pronounced (see parts e and f of Figure 3) at even shorter acquisition times (10 ms). In these panels the PHPs of rhodamine 6G and reserpine are 11 and 5.7 for the Hadamard mode and 0.6 and 0.4 for the conventional mode, representing improvements of 18 and 14, respectively. These improvements will be very useful in applications that require very fast acquisition rates.

Imaging Surface-Induced Dissociation and Postsource Decay. In addition to the multiplexing advantage[27] from 100% duty cycle, the imaging HT-TOFMS can image the ion beam profile at the detector and obtain mass spectra from every "pixel". If different chemical or physical processes are dispersed spatially, they will appear at different positions at the detector and extra information can be obtained. As a demonstration of the capability of the imaging HT-TOFMS, we have investigated the fragmented ions that underwent surface-induced dissociation (SID) inside the reflectron and the ions that fragmented spontaneously through postsource decay (PSD).

SID[28] is a fragmentation technique in tandem mass spectrometry where ions are forced to collide with a surface. Upon collision, some fraction of an ion's incident kinetic energy is converted into internal energy, which causes fragmentation. Some advantages of SID over collision-induced dissociation are greater energy transfer efficiency and better vacuum compatibility. In its most common implementation, the SID surface is mounted between two mass analyzers with a nonlinear[29,30] or linear[31] geometry. Several groups have performed SID in TOFMS by using a movable reflectron backplate as the SID surface.[32−34] The backplate, which is at the end of the reflectron for normal operation, can be moved very close to the reflectron entrance for SID experiments. Other groups have used the reflectron backplate that is fixed in position, but the SID fragments had to be pushed through the reflection using delayed extraction.[35,36]

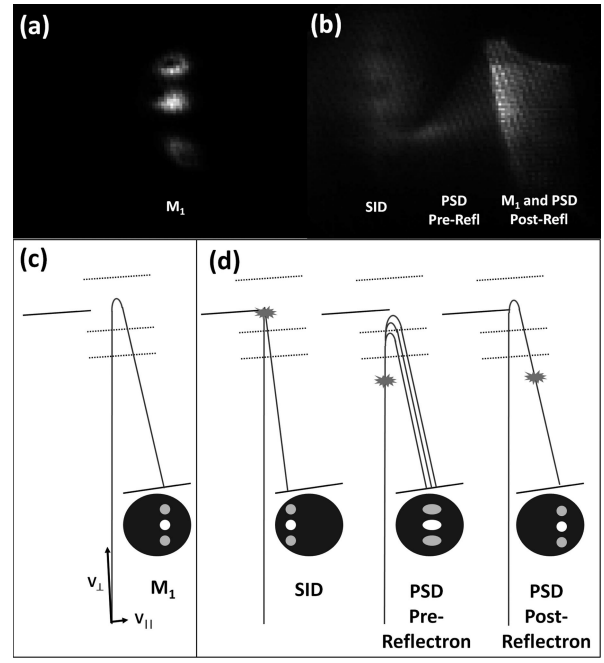

Figure 4. Two-dimensional images of triply charged angiotensin I (433 amu) with the SID surface (a) withdrawn and (b) inside the reflectron. Illustrations showing the trajectories and arrival patterns at the detector of (c) precursor ions and (d) three fragmentation processes: SID, PSD pre-reflectron, and PSD post-reflectron. PSD does occur inside the reflectron but is spread in position and time between pre- and post-reflectron PSD signals.

For the present work, a SID surface was mounted to one of the electrodes in the two-stage reflectron, which could be horizontally translated in and out of the ion beam path with a linear manipulator. Triply charged angiotensin I was used for all experiments. Most tandem MS techniques require precursor ion selection. By controlling the electrospray solution conditions and the ion source settings, we were able to generate an ion beam that when analyzed by MS showed only the triply charged angiotensin peak. In this manner we avoided the need for precursor selection.

Parts a and b of Figure 4 present the 2D images of x, y positions when the ion beam path is clear and blocked by the SID surface. Spatial separation of the different fragmentation processes along the x-axis happens inside the reflectron because the reflectron is horizontally rotated by 4° relative to the ion propagation direction. The velocity of an ion at the entrance to the reflectron can be divided into two components that are parallel ($v_{||}$) and perpendicular ($v_{\perp}$) to the reflectron electrodes, as shown in Figure 4c. The x position of ion arrival at the detector is given by the product of the parallel velocity component and the flight time because the parallel velocity component does not change upon fragmentation or deceleration/acceleration in the reflectron (except slight modification from kinetic energy released[37,38]).

(28) Dongré, A. R.; Somogyi, A.; Wysocki, V. H. *J. Mass Spectrom.* **1996**, *31*, 339–350.
(29) Wysocki, V. H.; Ding, J.-M.; Jones, J. L.; Callahan, J. H.; King, F. L. *J. Am. Soc. Mass Spectrom.* **1992**, *3*, 27–32.
(30) Schey, K.; Cooks, R. G.; Grix, R.; Wollnik, H. *Int. J. Mass Spectrom. Ion Processes* **1987**, *77*, 49–61.
(31) Galhena, A. S.; Dagan, S.; Jones, C. M.; Beardsley, R. L.; Wysocki, V. H. *Anal. Chem.* **2008**, *80*, 1425–1436.
(32) Williams, E. R.; Fang, L.; Zare, R. N. *Int. J. Mass Spectrom. Ion Processes* **1993**, *123*, 233–241.
(33) Williams, E. R.; Jones, G. C.; Fang, L.; Zare, R. N.; Garrison, B. J.; Brenner, D. W. *J. Am. Chem. Soc.* **1992**, *114*, 3207–3210.
(34) Maaijer-Gielbert, J. D.; Beijersbergen, J. H. M.; Kistemaker, P. G.; Weeding, T. L. *J. Mass Spectrom. Ion Processes* **1996**, *153*, 119–128.
(35) Haney, L. L.; Riederer, D. E. *Anal. Chim. Acta* **1999**, *397*, 225–233.
(36) Gamage, C. M.; Fernandez, F. M.; Kuppannan, F.; Wysocki, V. H. *Anal. Chem.* **2004**, *76*, 5080–5091.
(37) Cooks, R. G.; Beynon, J. H.; Caprioli, R. M.; Lester, G. H. *Metastable Ions*; Elsevier: Amsterdam, The Netherlands, 1973.

The perpendicular velocity component will change during deceleration/acceleration in the reflectron, and the flight time will change depending on the position of the fragmentation and the mass and charge of the fragment. As in Figure 4c, if an ion does not fragment or if it fragments after exiting the reflectron, it will reach the detector at high x position, farther to the right. If an ion fragments before or inside the reflectron, its flight time will be reduced and the fragments will arrive at the detector at a smaller x position, toward the left (Figure 4d). The flight time of a PSD fragmented ion is typically reduced because the kinetic energy is divided into two fragment ions upon fragmentation according to the ratio of their masses. Thus, fragment ions are reflected by the reflectron at an earlier stage (lower potential) due to reduced kinetic energy per unit charge. For fragmentation of multiply charged ions where the fragment ion has a large mass and a different charge from the precursor ion, the kinetic energy per unit charge will be greater. In this case, the PSD fragment will arrive at the detector after the flight time expected for its precursor.

Thus, for PSD fragments, the position x and the flight time t will be highly correlated with a slope given by the parallel velocity component. The x position will deviate from this correlation if an ion collides with the SID surface because it will lose most of its kinetic energy upon collision. Its new velocity will be determined by the interaction with the surface. Then, it will be reaccelerated in a direction perpendicular to the surface reaching the detector at a lower x position (Figure 4d). Therefore, SID and PSD fragment ions will have very different correlations between x and t, which allows us to study these two processes separately.

The 2D ion image recorded on the detector with the surface withdrawn is shown in Figure 4a, and this process is pictured schematically in Figure 4c. The three branches of the Hadamard modulated ion beam are visible. As the SID surface is moved into the reflectron, the initial beam is clipped from the left and three new, displaced ion beam branches begin to appear, as shown in Figure 4b. Also apparent is a tailing process that we assign to PSD. Hence, we see in Figure 4b three ion populations that have been assigned from the left to SID fragments, PSD fragments, precursor ions, and precursor ions that underwent PSD after the reflectron. The latter two overlap. These different processes are explained schematically in Figure 4d. Precursor ions are visible on the right side because the surface did not completely block the ion beam path.

The 3D histogram (x, y, t) for SID collision voltage of 30 V (Figure 4b) were deconvoluted with Hadamard sequence along the time axis, and the image cross-sections at various flight times are shown in parts b−f of Figure 5, where positive and negative intensities are displayed as red and blue, respectively. Recall that a negative intensity represents a negative cross correlation with the Hadamard sequence. Characteristic Hadamard deflection patterns of negative−positive−negative beams are seen at different positions in the images with quite different flight times. Figure 5a is the 2D image of the ion counts, the same as shown in Figure 4b, for comparison.

A 2D plot of the x position and flight time is shown in Figure 6a. The PSD fragments lie inside the dotted box, where the x position and flight time have a linear correlation with a slope of

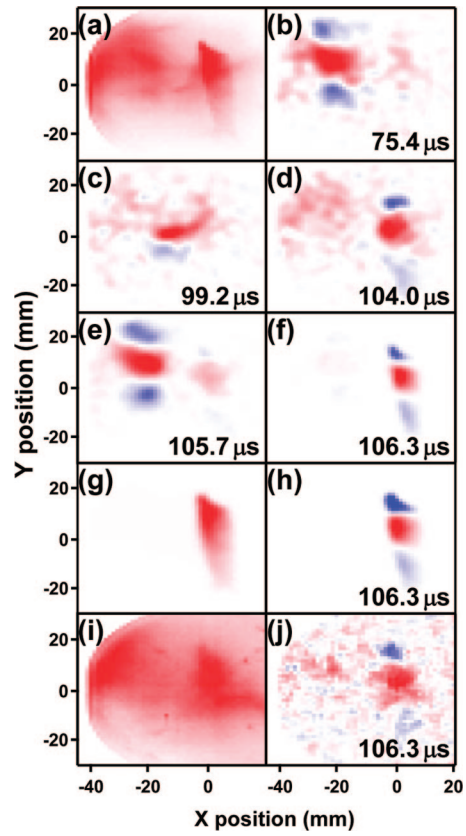

Figure 5. Angiotensin I undergoing SID at a collision energy of 90 eV: (a) *xy* image of total ion counts summed over time and (b−f) *xy* images at different flight times at a detector grid at 0 V. SID is apparent in parts b and e, PSD is apparent in parts c and d, and the precursor ion appears in part f. The detector grid is at 1500 V in parts g and h and 2000 V in parts i and j where parts g and i are the ion counts summed over time, and parts h and j are images at flight times that only show the precursor ions.

1800 m/s. This velocity is the expected parallel velocity component of triply charged angiotensin I, which is calculated from an acceleration voltage of 1500 V and a 4° rotation of the reflectron. The most intense peak inside the dotted box at 106.3 μs is from the precursor ions. There are two other intense peaks outside the box at an x position of −21 mm and flight times of 75.4 and 105.7 μs, tentatively assigned to histidine immonium at 110 amu and doubly charged angiotensin I at 649 amu. The x position is the same for the two peaks suggesting that most of the kinetic energy of the ions has been lost upon collision with the SID surface. The *xy* images of the two SID fragments (Figure 5b,e) are moderately broader than that of the precursor ions at 106.3 μs (Figure 5f). We attribute this behavior to the angular distribution of the ions off the surface. The flight time spectrum obtained by summing over x positions (Figure 6b) would be the mass spectrum expected from an SID experiment using a TOFMS without an imaging detector. Note that most of the PSD fragments are hidden in the baseline and also the precursor ion at 106.3 μs and the SID fragment at 105.7 μs are shown as a single peak. The peaks inside the dotted box were summed over x position, and the flight time spectrum is shown in Figure 6c, which is the spectrum of PSD fragments that are normally not visible in electrospray mass spectrometers. In our setup, before collision with the surface, PSD happens from the precursor ion beam with a small probability from the tail of the internal energy distribution.

(38) Laskin, J.; Lifshitz, C. *J. Mass Spectrom.* **2001**, *36*, 459–478.

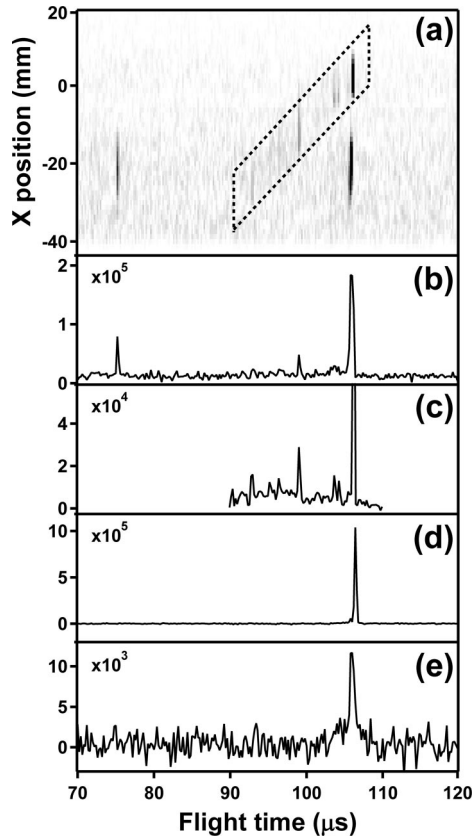

Figure 6. Mass spectra for data presented in Figure 5: (a) 2D plot of *x* position and flight time with the detector grid at 0 V in which the PSD fragment ions lie within the dotted box and (b−e) flight time spectra obtained (b) by summing over *x* positions, (c) by summing the dotted box region over *x* positions, (d) with detector grid at 1500 V, and (e) with detector grid at 2000 V.

Upon collision, a large fraction of the ion beam is neutralized and a small fraction (∼5%) undergo SID. Thus, PSD signal is enhanced relatively. Then, PSD signal is isolated from the more intense SID peaks by using different $x-t$ correlations. Thus, we are able to observe them because a large fraction of the precursor ions are neutralized and the PSD ions have been separated from other intense peaks.

To confirm that the ions centered at 0 mm are uncollided ions and the ions at small *x* position, less than −20 mm, are fragmented ions, we repeated the experiment with the voltage on the grid in front of the detector at 1500 V relative to the flight chamber, which is the same voltage used for acceleration of the ions. The SID surface is at a potential lower than 1500 V so ions that undergo SID will have energies per unit charge less than 1500 V and will not appear at the detector. As noted above, some ions that undergo PSD may have more kinetic energy per unit charge and arrive at the detector under these conditions. The assignment of ions that arrive on the left of the detector to SID fragments is clearly shown in Figure 5g, where all the ions at smaller *x* positions have been removed. After Hadamard deconvolution, the mass spectrum shows a single peak at 106.3 μs (Figure 6d). The *xy* image at this flight time is in Figure 5h, which is identical to the image at the same flight time when the grid voltage was zero (Figure 5f). We assign this image to the precursor ions.

We also repeated the experiments with the grid in front of the detector at 2000 V, which is higher than the reflectron backplate voltage of 1900 V. Because the grid is set to a voltage above the back plate of the reflectron, ions that have enough kinetic energy to pass the grid will not be reflected by the reflectron. At this setting, all ions reflected by the reflectron will be blocked and only neutral molecules will be detected (Figure 5i). Closer inspection of Figure 5i reveals a broad smear at small *x* positions, which come from neutrals generated by SID, and a broad smear at high *x* positions, which come from neutrals generated by PSD. The neutrals generated by SID will not be accelerated by the reflectron and will have a small velocity. Also, the neutrals generated by PSD inside the reflectron will have a small velocity with a continuous distribution depending on the position of the fragmentation. Thus, for these neutrals, the Hadamard modulation will be blurred out in time. If PSD happens before the reflectron, the neutral molecules will be traveling away from the detector and will not reach the detector. If PSD happens after exiting the reflectron, the velocity will not change and the neutral molecules will maintain the timing from Hadamard modulation. The mass spectrum of the ions at high *x* position has a single broad peak at 106.3 μs (Figure 6e). The *xy* image at this flight time also has the Hadamard modulated ions at high *x* position (Figure 5j), which shows that PSD is happening after the reflectron. The same study was repeated at a higher collision voltage (80 V), and the results are similar to what is presented in Figures 5 and 6 but show more SID peaks.

One requirement for Hadamard imaging is that the Hadamard modulation must be maintained during the fragmentation processes. The neutral molecules that are created at collision with the surface will not be accelerated by the reflectron and will lose the timing information. Some of these molecules will reach the detector, but will only contribute to the background noise. The modulation efficiency for the SID processes is low at about 25% compared to 90% for the precursor beam. This loss in modulation efficiency is mainly from the presence of neutral molecules and spread from the SID process. Because the 5 MHz Hadamard modulation (200 ns time bin) is maintained during SID and there is no tailing of the SID peaks, these images suggest that the surface-induced dissociation happens within about 200 ns. This conclusion is consistent with the results from the SID kinetics experiment by Gamage et al.[37]

Presently, the spatial resolution of the imaging HT-TOFMS is about 100 μm, but the images are much poorer, which is caused by the size of the ion beam. Future improvements in ion beam collimation optics at the ion source should markedly increase the image resolution. Also, the mass resolution is determined by the Hadamard modulation rate of 5−50 MHz and is typically a few hundred to a thousand. Nevertheless, the present resolution in space and time is sufficient to allow us to observe SID and PSD processes.

CONCLUSIONS

We have developed an imaging TOFMS with a 100% duty cycle based on pseudorandom ion beam modulation and 3D ion detection (*x*, *y*, and *t*). The use of an imaging detector to visualize the ion beams facilitates the optimization process, and high modulation efficiency can be easily achieved. Also by choosing the best windows in the data processing step, correlated noise between the channels could be removed to maximize the multiplexing advantage of the imaging HT-TOFMS. These advan-

tages were demonstrated by the increased peak height precision at short acquisition times (down to 10 ms). We believe that these advantages will prove useful in solution kinetics or chromatography experiments.

In addition to the multiplexing advantage, the imaging HT-TOFMS can provide mass spectra at every "pixel" of a 2D image. We have imaged the fragmented ions that underwent surface-induced dissociation inside the reflectron and the ions that fragmented spontaneously through postsource decay. These fragmentation processes showed very different correlations between x position and flight time and could be analyzed separately. The modulated ions maintain the Hadamard time-stamping during different fragmentation methods including PSD and SID. In this manner we are able to observe PSD in ions coming from electrospray.

ACKNOWLEDGMENT

This work was supported by the United States Air Force Office of Scientific Research (AFOSR Grant FA9550-04-1-0076). The authors thank Prof. Vicki Wysocki and her collaborators at the University of Arizona for kindly donating 2-(perfluorodecyl)-ethanethiol and a protocol for preparing thiol-modified surfaces.

Received for review July 18, 2008. Accepted September 2, 2008.

AC801512N